Author´s accepted manuscript
The manuscript accepted to publication in
IEEE International Conference on Mechatronics (ICM2021)

Frequency-domain experimental setup for mechatronic and suspension system components

Rafael Tavares
University of Agder (UiA)
Grimstad, Norway
rafael.tavares@uia.no

Michael Ruderman
University of Agder (UiA)
Grimstad, Norway
michael.ruderman@uia.no

***Abstract*—This paper presents a frequency-domain experimental setup for modal analysis of mechatronic and suspension system components. Design, instrumentation and dynamic behavior of the one degree-of-freedom (DOF) system, capable of providing both, periodic and application-specific, excitation forces is described. The excitation is realized by an electromagnetic modal shaker with additional assembly and interface components designed and instrumented for frequency-domain analysis of vertical dynamics. Frequency response functions (FRFs) of the implemented system are experimentally measured and the associated basic model parameters are calculated, correspondingly identified. Accurate fit between the measured FRFs and modeled dynamics is shown for sufficiently large frequency range 0.1–30 Hz of the mechanical system response. Exemplary standard road profile excitations are also conducted to demonstrate the applicability of the designed system for frequency-domain testing of components in the vehicle suspension systems.**

***Index Terms*—mechatronics, system identification, systems and signal analysis, modal testing, instrumentation**

I. Introduction

Experimental study of structural dynamics provides a major contribution to understand and cope with the many vibration phenomena [1], [2]. Increasing demands of safety and reliability of the embedded mechatronic parts, especially where the varying and broadband loads are involved, require a better understanding of dynamic properties and response of those components, also within whole assembly. Modal testing techniques have been used for decades for determining the nature and extent of vibration response levels, e.g. measurement of the material properties under dynamic loading, such as damping capacity, vibration decompositions [3], and structural health monitoring and fatigue endurance [2]. Recall that the objectives of modal testing are in determining modal properties for a structure, among which are the natural frequencies, damping factors, and mode shapes [2]. Via signal analysis, the vibration response of the test subjects, or specimens, under controlled laboratory conditions is measured and transformed into frequency response functions (FRFs), mostly using Fast Fourier Transformation (FFT) techniques. Typical excitation signals can be impulses, sequential sinusoids and alternatively multisine signals, swept sine or chirp, and others.

Modal analysis has numerous practical applications and, in particular, essential investigations have been often reported for aeronautical and automotive e.g. [4], civil e.g. [5] and mechanical e.g. [2] engineering. In automotive engineering, apart from structural design and safety aspects, the suspension systems and their multiple mechatronic components are of keen interest. Comfort and road-handling performance of ground vehicles are mainly determined by the damping characteristics of the suspension systems, either passive, semi-active or active [6], [7]. Widespread state-of-the-art approaches in suspension system design have been relying on the quarter-car model for describing the interactions between the suspension system, the tire and the chassis in a single corner of a vehicle. It represents only the vertical motion of vehicle body and wheel, hence the vertical dynamics of vehicles can be easily investigated by using such models [6], [8]. Due to research conduct on improving the road performance of suspension systems, and also due to a continuing increase in the efficiency and compatibility of integrated and embedded mechatronic systems in automotive, more and more innovative and original technologies emerged as available for active and semi-active suspension systems [9].

The development and prototyping of these new concepts is well tied along with several experimental studies to prove the feasibility and reliability of such innovative system, even in a reduced scale, as reported in [10]. Quarter car test rigs are commonly used for the study and design of active and semi-active suspensions. Most of the experimental setups consist of a wheel, a sliding cantilever representing a quarter of a car body mass, and in between a spring and an active damper with bushing and respective links, cf. [10]–[14]. Although being able to support the full corner of a ground vehicle, the adherent increased complexity of having the full corner suspension leads to added difficulties in characterizing the experimental setup: the necessity to account geometric non-linearities, the precondition of using accurate tire models, having a higher number of system parameters to identify, more model uncertainties, to name a few, cf. [12]. This leads to a more difficult and complex task on identifying such extensive setup, especially when the main research question remains to evaluate and test new mechatronic components in the early development stages and prototyping of active or semi-active suspension. For this reason, often a reduced structure is used for identifying frequency-domain characteristics and for mitigating effects of other existing sub-dynamics, process noise or model uncertainties [14].

This paper aims to present the design, implementation, and

experimental validation of a one degree-of-freedom (DOF) frequency-domain experimental setup intended to perform modal testing of mechatronic components, especially those to be employed in suspension systems. The proposed experimental setup addresses necessity of reducing system complexity for testing vertical dynamics of individual components of interest of the suspension column, e.g. integration of functional materials in suspension systems. Particular focus was given to the flexibility and modularity of the setup, in order to allow for reconfigurability and, this way, frequency response and modal analysis of different specimens and mechatronic subassemblies. The measurement and estimation of the frequency response characteristics, see e.g. [15] for basics, of the experimental setup self is of prior focus in this work.

The rest of the paper is organized as follows. A detailed description of the experimental setup and its main components are provided in Section II. Section III, as main part, discusses the system dynamics along with experimental measurements and estimation of the FRFs of interest. Frequency-domain analysis of the experimental measurements conducted to evaluate the performance and feasibility of reproducing the standard road profiles are presented in Section IV. At the end, final conclusions are provided in Section V.

II. System design and instrumentation

The experimental setup, shown in Fig. 1, was designed as 1-DOF system, in first line, for testing components in vertical dynamics configuration. The design focuses on frequency-domain study of mechatronic parts and elements placed in between the sprung/unsprung mass and controllable excitation. The main requirements on the experimental setup are: having similar dynamic behavior in terms of natural frequency of the scaled down sprung mass; vertical guided movement of the chassis mass with ideally low friction disturbance; capability of applying realistic excitation, like those from the standard road profile kinematic signals.

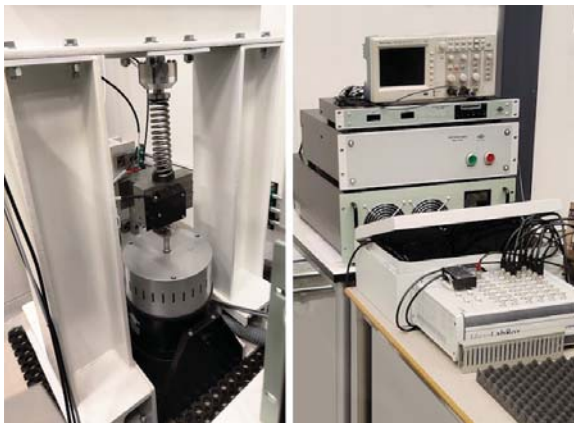

Fig. 1: Laboratory apparatus of the experimental setup and powering, sensing, and control electronics.

The system main components are schematically presented in Fig. 2, based on the designed CAD technical drawing of the entire assembly. A moving carriage ②, correspondent

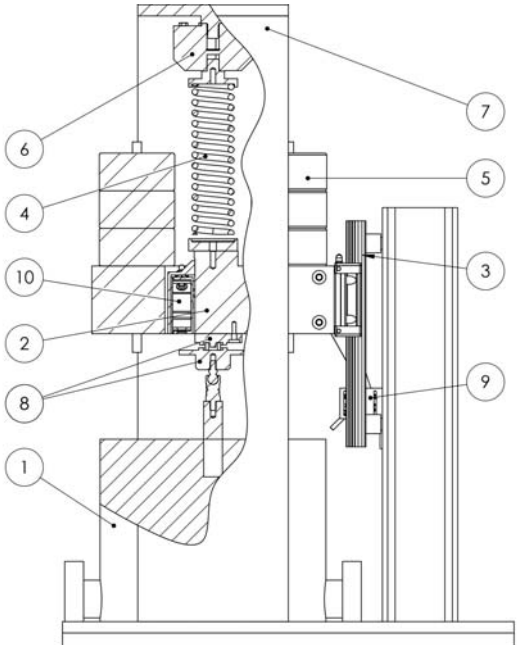

Fig. 2: Schematic representation of the setup components.

to the unsprung mass of the vehicle, is excited from the bottom side by a modal shaker ①. The vertical motion of the moving carriage ② is supported by a linear four-row circular-arc contact HIWIN guide-way ③. This linear guide-way was chosen so as to minimize disturbing friction of the vertical guidance of the chassis mass. A compression spring ④, representing the scaled stiffness k of a passive suspension, is placed in between the force sensor ⑥ (HBM U10M-2.5kN), which is fixed at the top beam of mechanical frame, and the moving carriage. Optionally, additional masses ⑤ can be stacked on top and clamped to the moving carriage in order to adjust the unsprung mass m. Together with using different compression springs (of different stiffness k) this allows to adjust the natural frequency $\omega_0 = \sqrt{km^{-1}}$ of the system.

The force excitation is given by an electromagnet-based modal shaker (Brüel & Kjær type 4828) with a force rating up to 1000 N suitable for impulse, sinusoidal, and random signals with a wide frequency range (up to 5000 Hz) and a peak-to-peak displacement up to 50.8 mm. This transducer is driven by a dedicated field power supply and a power amplifier that conditions the current and voltage for the modal exciter according to the reference control signal. The power amplifier allows for monitoring the modal exciter's current and voltage. A DC static centering unit provides the armature "suspension" and is responsible for the correct positioning of the shaker rod relative to the exciter's housing ("zero-positioning").

The system's modularity and configuration flexibility are important characteristics that were taken into account during the design process, in order to allow for testing of different suspension components and mechatronic devices. The moving carriage consists of two big steel blocks connected by two side steel plates. This allows the ability to access and reconfigure the sensors mounted on the moving carriage. The adapter

couplings (8) placed on the bottom of the moving carriage and modal shaker rod are interchangeable and allow for varying size and shape specimens and components. Here it is worth noting that inclusion of piezoelectric stacks into semi-active suspension systems [16] is of particular interest in our recent and future studies.

The mechanical frame (7) was built around the modal shaker fixture using IPE steel beams. The single criteria for beam dimensioning was requiring that the elastic bending in the middle of the top beam is one order of magnitude below the smallest displacement to be measured in the specimen at maximum excitation force. That was verified through finite element model (FEM) simulation. The overall beam size was then additionally increased, in order to increase the overall weight of assembly.

An optical laser sensor (9) (Micro-Epsilon optoNCDT 1420-50) is placed on side of the structure frame to measure the displacement of the moving carriage without contact. A higher precision laser triangulation sensor (10) (Micro-Epsilon optoNCDT 2300-2) is fixed within the moving carriage, in order to measure additionally the micro compressions, correspondingly elongations, of the mechatronic component under testing. Due to the small mangitude of compressions measured, the mechanical rigidity of structural coupling parts and proper locking of adjustment bolts are ensured to achieve reproducibility of measurements.

The dSpace MicroLabBox (DS1202) is used to generate the reference control input signal U, provided to the modal shaker, and for data acquisition through the BNC analog input ports, with all signals being sampled at 10 kHz. A dedicated embedded circuit enables the laser sensors through the dSpace MicroLabBox digital I/O ports.

III. Dynamics and FRF responses

The experimental system dynamics are evaluated in frequency domain, including: identifying dynamics response of the system, i.e. the transfer functions of interest; designing the appropriate excitation signals; measurement and estimation of the system FRFs and identification of the remaining model parameters, which are not available from data sheets and/or CAD and FEM calculations.

A. System dynamics

Due to a broad frequency range of the shaker, one can assume sufficiently low time constants of the electric and electro-magnetic circuits, which can then be neglected when comparing with time constants of the mechanical components in place. Considering the excitation force signal F_A of the modal shaker, one can assume that this is linearly proportional to the current I of the shaker coils, so that

$$F_A \propto k_a I, \tag{1}$$

where k_a is the current-to-force constant. The moving carriage can be defined as the second-order system, with the corresponding transfer function

$$\frac{X(s)}{I(s)} = \frac{k_a}{ms^2 + bs + k}, \tag{2}$$

where X is the measurable position of the moving mass m, k is the stiffness of the compression spring, and b is the overall viscous damping. By convention, s is the Laplace variable, while for referring to the measured frequency response functions the $j\omega$ argument is used. Here ω is the angular frequency, and j is the imaginary part of complex numbers.

Another transfer function of interest is the relationship between the modal shaker current I, i.e. proportional to the excitation force, and the measured force F which is propagated up through the overall mechanical structure. Recall that the force sensor for F is fixed at the top of the structure frame, cf. Fig. 2. Due to parallel spring-damper configuration of the second-order dynamics (2), the Kelvin-Voigt, see e.g. [17], force transducer is an inherent assumption for capturing F in response to F_A-propagation through the structure. This results in the transfer function

$$\frac{F(s)}{I(s)} = k_a \cdot \frac{(bs + k)}{ms^2 + bs + k} \cdot \frac{1}{\tau s + 1}, \tag{3}$$

while an additional non-modeled first-order subdynamics, with time constant τ, is added for keeping the phase shift constraints out from the measured characteristics. Since the moving carriage mass m and the spring stiffness k are known, from CAD/FEM design, only the k_a, b and τ parameters need to be identified from the measured FRFs.

B. System excitation

An often used excitation signal for identifying frequency response of the system is a swept-sine test signal, also referred to as a chirp signal, see e.g. [15]. The signal constitutes a sine wave where the frequency is linearly increasing as function of time. This leads to the modal shaker command input

$$U = A \sin(2\pi f(t) t), \tag{4}$$

where A is the chirp gain, and the time-varying frequency is given by

$$f(t) = f_0 + \frac{f_1 - f_0}{2T} t. \tag{5}$$

The used chirp signal was set for the frequency range $f_0 = 0.1$ Hz, $f_1 = 100$ Hz and the runtime $T = 300$ s. This way, the system is smoothly excited over the whole frequency range, and the magnitude and phase are afterwards computed as the ratio of the output Fourier transformation to the input Fourier transformation of the measured time series. For the sake of better visualization, a high-dimension Hamming window is also applied to the Fourier transformed data. It is worth noting two main limitations of the chirp signal in system identification: the transient dynamics are (partially) present in the FRFs, due to continuous increase of the excitation frequency; and the number of excitation cycles for lower frequencies is lower than for the higher frequencies.

Alternatively, the frequency response measurements with periodic test signals allow for determining the relevant frequency range by the discrete (sampled) points in the frequency spectrum [15]. Typically sinusoidal signals at fixed frequencies are used, with the experiment being repeated for each

frequency ω_v of interest. A time series consisting of the set of sinusoidal waves of different frequencies applied one after another is commonly used in practice for system identification. Then, considering $G(j\omega) = Y(j\omega)/Z(j\omega)$ for each ω_v realization of a non-parametric model from input $Z(j\omega)$ to output $Y(j\omega)$, the amplitude and phase are determined by

$$|G(j\omega_v)| = \frac{y_0(\omega_v)}{z_0(\omega_v)}, \qquad \angle G(j\omega_v) = -t_\phi \omega_v. \tag{6}$$

Here t_ϕ denotes the time duration of the phase lag between the output $y(t)$ and input $z(t)$ measurement. Correspondingly z_0 and y_0 are the bias-free maxima (i.e. amplitude) of the input steady-state output oscillations.

C. Frequency response function measurement and estimation

First, the FRF measurements were accomplished by exciting the system with the chirp signal (4)-(5).

Then, the discrete point measurement over the frequency spectrum was also implemented by sequentially exciting the system with a sinusoidal input of different frequencies, within the range of interest. These FRFs were computed for total of 180 frequency points, equidistantly distributed on the logarithmic scale within the [0.2, 100] Hz frequency range. A total of 10 periods for each frequency w_v were used, where the first 3 are skipped as transient periods and the remaining 7 are used as estimation periods.

From the measured signals it is also possible to verify some characteristics of the system. Those are the amplification gain factor of the low-level controlled shaker $|V(j\omega)/U(j\omega)| = 29.26$ dB, where V is the shaker control voltage, and the stiffness of the spring, which is resulting from the following amplitude response $|F(j \cdot \omega_{\min})/X(j \cdot \omega_{\min})| \approx 17.34$ kN/m.

The obtained from the measured data frequency response functions for input and output pairs of interested are shown in Figs. 3-6, that for both the chirp and set of sinusoid signals. The frequency response of the identified transfer functions (2) and (3), with the determined parameters listed in Table I, is shown over the measurements. For parameter estimation, the computed discrete points in the frequency spectrum for magnitude and phase are used based on the set of sinusoids.

It is visible that the set of sinusoid identification signals provides a better (i.e. more accurate) dynamics signature at lower frequencies, while the oscillation from transients in the chirp are apparent. Note that sinusoid identification implies, however, higher experimental costs (time) when compared to the chirp signal. The peak amplitude is observed in the frequency responses $X(j\omega)/I(j\omega)$ and $F(j\omega)/I(j\omega)$ (Fig. 3 and Fig. 4) for the frequency $f \approx 4.4$ Hz, disclosing a resonant behavior which is consistent with the natural frequency of the mechanical system ω_0. From (2) and (3) one can conclude that beyond the frequency ω_0, there is a decreasing slope by -40dB per decade in $|X(j\omega)/I(j\omega)|$ and $|F(j\omega)/I(j\omega)|$, due to the relative degree two of the system in both cases. This is also visible in $-180°$ asymptote of the phase response. The well visible but not modeled higher-order, correspondingly - frequency, dynamics is up from about 30 Hz.

TABLE I: Computed and identified model parameters

Parameter		Computed value	Identified value	Units
m	Moving carriage mass	22.2426	-	kg
b	Damping coefficient	-	134.86	Ns/m
k	Spring stiffness	17000	-	N/m
k_a	Current-to-force gain	-	24.1744	F/A
τ	Time constant	-	0.01	s

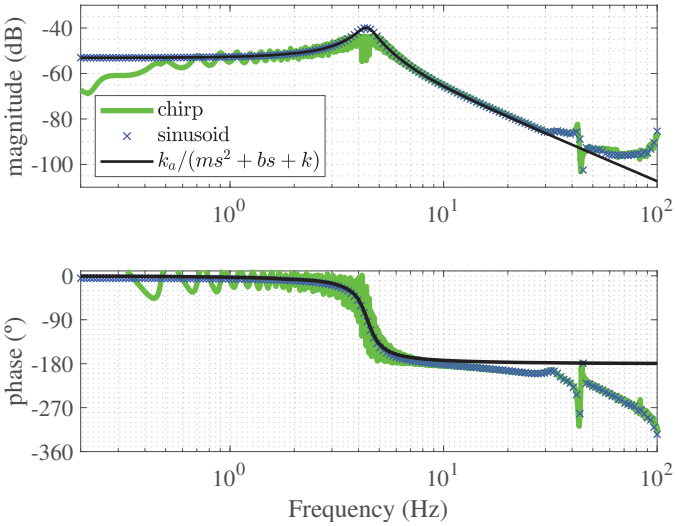

Fig. 3: Measured frequency response function: $X(j\omega)/I(j\omega)$.

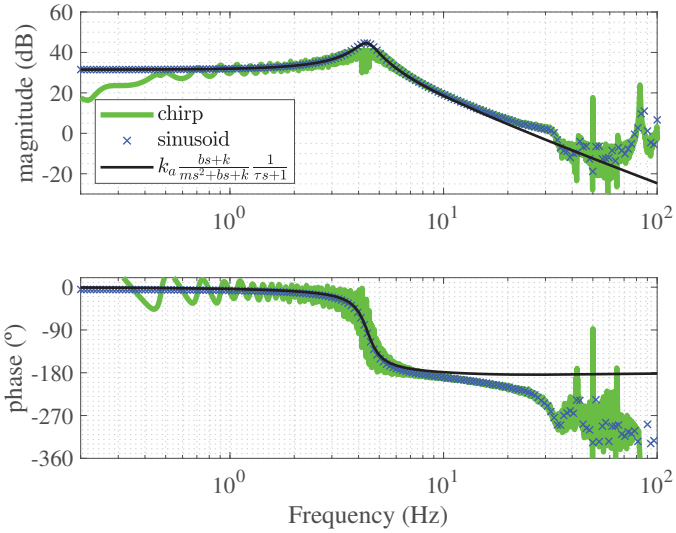

Fig. 4: Measured frequency response function: $F(j\omega)/I(j\omega)$.

The $F(j\omega)/U(j\omega)$ response shown in Fig. 5 discloses the capability of propagated force excitation for the given configuration ω_0. The continuously decreasing (with increasing frequency) gain factor should be, however, taken into account when designing the excitation profiles for application-specific command $U(j\omega)$. To show flexibility and adaptability of

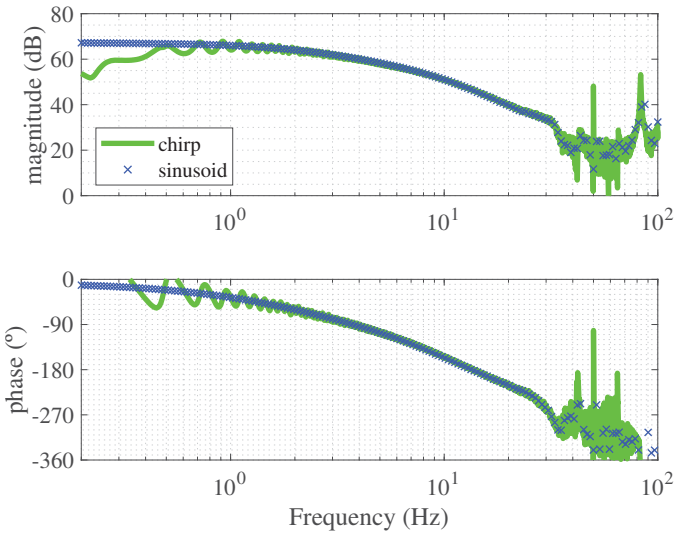

Fig. 5: Measured frequency response function: $F(j\omega)/U(j\omega)$.

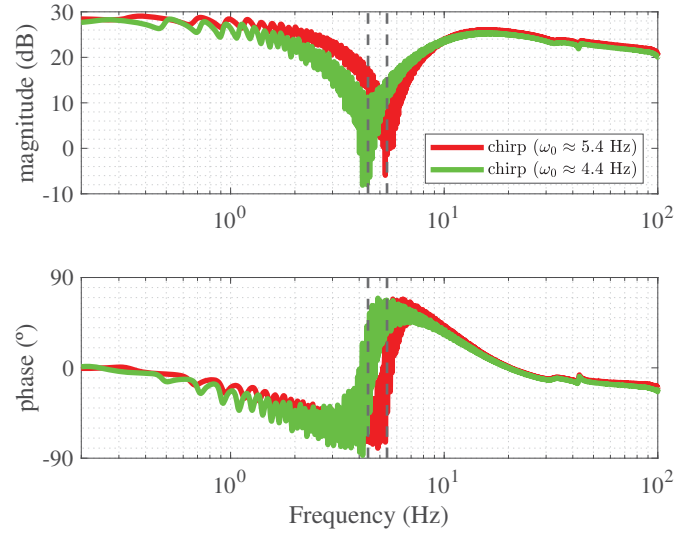

Fig. 6: Measured frequency response function: $I(j\omega)/U(j\omega)$.

the system, Fig. 6 demonstrates the measured $I(j\omega)/U(j\omega)$ response to the chirp excitation signals for two different mass/spring configurations: the nominal one with parameters shown in Table I and natural frequency $\omega_0 = 4.4$ Hz; and the adjusted configuration with higher spring stiffness resulting in natural frequency $\omega_0 = 5.4$ Hz. One can see an apparent shift of the anti-resonance peak, corresponding to ω_0, marked for both configuration. From this FRF, it is visible that the internal controller of the modal shaker is partially compensating for the resonant behavior of mechanical system with bounded motion.

Focusing on dynamics of the moving carriage, the mass acceleration $\ddot{x}(t)$ can be assessed by double discrete derivative of the relative displacement. A low-pass filter (LPF)

$$H(s) = \frac{\omega_c}{s + \omega_c}, \tag{7}$$

with cut-off frequency $\omega_c = 2\pi \cdot 200$ rad/sec was, however, additionally used to smooth the obtained signal. The same LPF is also applied to the current signal $i(t)$ to compensate for the introduced phase lag. The frequency response for $\ddot{X}(j\omega)/I(j\omega)$ is shown in Fig. 7, together with the corresponding transfer function. This allows for further analysis of suspension components since, in a sprung-unsprung dual mass configuration, the vertical acceleration of the sprung mass is usually used to evaluate the ride comfort performance.

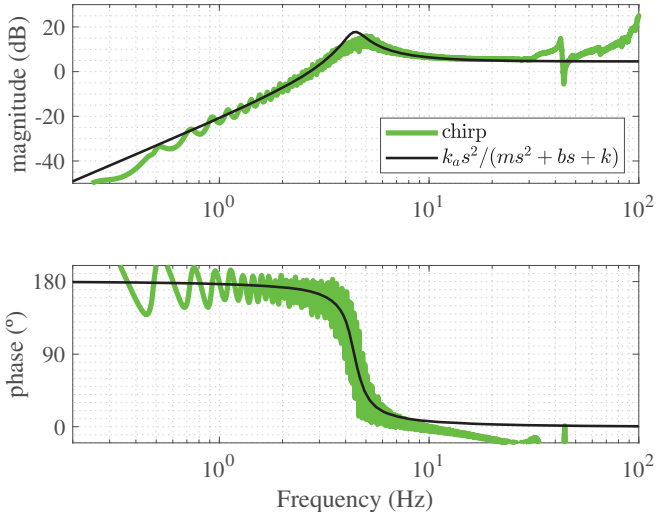

Fig. 7: Measured frequency response function: $\ddot{X}(j\omega)/I(j\omega)$.

IV. Standard Road Profile Excitation

The proposed experimental setup has in focus the suspension system applications, among others, envisaging future studies which involve modal testing of prototyped mechatronic components, mainly for system identification, but also energy harvesting and suspension control purposes. As seen in previous works, the frequency range of interest in vehicle suspensions is mostly within 0.1-40 Hz, cf. with [6], [9], [18].

From more realistic applications' point-of-view, it is of interest to see the response of the experimental setup to standardized road profiles. Nowadays, synthetic longitudinal road profiles based on ISO 8608 road classification are often used for simulation purposes [19]. This road excitation can be characterized as a specifically filtered Gaussian band-limited white-noise. A standard road excitation, according to ISO 8608 classification, can be then generated as a white-noise signal processed through the filter

$$G_e(s) = \frac{\sqrt{2\pi r \nu}}{s + \omega_r}. \tag{8}$$

Here r is the road roughness coefficient, ν is the longitudinal velocity of the vehicle, and ω_r is the road cutoff frequency. For a detailed description of generating standard road profiles we refer to previous works [16], [18]. The resulted road displacement W, out from the filtering (8), is then applied to the reference command U, as a force transmitted by the vehicle tire, resulting in

$$\frac{U(s)}{W(s)} = k_a^{-1}(b_t s + k_t). \tag{9}$$

The tire damping and elastic coefficients, b_t and k_t respectively, are assumed as in [16].

To evaluate the capability of exciting the system by the typically good-paved surfaces (Class A, typically motorway) and rather lower quality paved surfaces (Classes B and C for local highways and city roads), correspondent control input signals U for the modal shaker were generated. The vehicle is considered to be riding at a constant longitudinal velocity of $\nu = 100$ km/h for the class A, $\nu = 70$ km/h for the class B and $\nu = 50$ km/h for the class C, reference velocity values for each road according to [19].

Measured frequency response function $F(j\omega)/I(j\omega)$ for standard road excitation profiles is shown in Fig. 8. One can observe an increase of the magnitude as the rough roughness r increases, consistent with higher kinematic excitation, and correspondingly excitation forces, due to lower road quality. Strong attenuation of the resonance peaks, otherwise observed before in Fig. 4, is due to lower excitation magnitudes (bringing out additional nonlinearities and couplings), power dispersion over the whole frequency range (white-noise type power source), and additional pre-filtering of the input signal, both from the road cutoff frequency and the tire damping term.

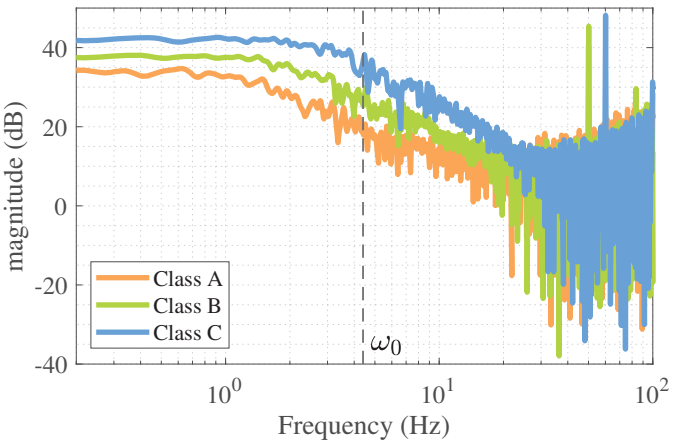

Fig. 8: Measured frequency response function $F(j\omega)/I(j\omega)$ for road excitations ISO 8608 class A, B and C.

V. Conclusions

An experimental setup for frequency-domain analysis of different mechatronic and, especially, suspension system components is reported. The initially assumed system dynamics were experimentally measured, FRF computed and analyzed. The fitted parametric transfer functions coincide accurately, to the large extent, with the experimentally measured responses that argues for validity of results, system specification, and initial assumptions. Additional process noise and unmodeled higher-order dynamics are also clearly visible in the measured FRFs for frequencies higher than 30 Hz.

The capability of controlling and reproducing excitation signals over the desired frequency range for a particular application of interest, i.e. vehicle suspension systems and their mechatronic elements, shows the feasibility of using the designed system for frequency-domain identification, analysis and dynamics evaluation, and further use for testing and validation of models and control prototypes. Here, especially, the reconfigurability and instrumentation of the moving carriage which can be excited by real (measured) road profiles disclose potential for investigations of passive, active and semi-active suspension components, including those with integration of functional materials and with further goal of an additional energy harvesting.

Acknowledgment

This work has received funding from the European Union Horizon 2020 research and innovation programme H2020-MSCA-RISE-2016 under the grant agreement No 734832.

References

[1] W. Heylen, S. Lammens, P. Sas *et al.*, *Modal analysis theory and testing*. Katholieke Universiteit Leuven Leuven, Belgium, 1997, vol. 200, no. 7.

[2] D. J. Ewins, *Modal testing: theory, practice and application*, 2nd ed. John Wiley & Sons, 2009.

[3] M. Feldman, *Hilbert transform applications in mechanical vibration*. John Wiley & Sons, 2011.

[4] B. Peeters, P. Guillaume, H. Van der Auweraer, B. Cauberghe, P. Verboven, and J. Leuridan, "Automotive and aerospace applications of the polymax modal parameter estimation method," in *Proceedings of IMAC*, vol. 22, no. 1, 2004.

[5] C. Rainieri and G. Fabbrocino, "Operational modal analysis of civil engineering structures," *Springer, New York*, vol. 142, p. 143, 2014.

[6] S. M. Savaresi, C. Poussot-Vassal, C. Spelta, O. Sename, and L. Dugard, *Semi-active suspension control design for vehicles*. Elsevier, 2010.

[7] P. S. Els, N. J. Theron, P. E. Uys, and M. J. Thoresson, "The ride comfort vs. handling compromise for off-road vehicles," *Journal of Terramechanics*, vol. 44, no. 4, pp. 303–317, 2007.

[8] D. Karnopp, "Active damping in road vehicle suspension systems," *Vehicle System Dynamics*, vol. 12, no. 6, pp. 291–311, 1983.

[9] H. E. Tseng and D. Hrovat, "State of the art survey: active and semi-active suspension control," *Vehicle system dynamics*, vol. 53, no. 7, pp. 1034–1062, 2015.

[10] G. Koch and T. Kloiber, "Driving state adaptive control of an active vehicle suspension system," *IEEE transactions on Control Systems technology*, vol. 22, no. 1, pp. 44–57, 2013.

[11] F. Svaricek, T. Fueger, H.-J. Karkosch, P. Marienfeld, and C. Bohn, "Automotive applications of active vibration control," *Vibration Control*, pp. 303–318, 2010.

[12] C. Lauwerys, J. Swevers, and P. Sas, "Robust linear control of an active suspension on a quarter car test-rig," *Control Engineering Practice*, vol. 13, no. 5, pp. 577 – 586, 2005.

[13] C. Zauner, J. Edelmann, and M. Plöchl, "Modelling, validation and characterisation of high-performance suspensions by means of a suspension test rig," *International Journal of Vehicle Design*, vol. 79, no. 2-3, pp. 107–126, 2019.

[14] M. Gobbi, P. Guarneri, G. Mastinu, and G. Rocca, "Test rig for characterization of automotive suspension systems," *SAE International Journal of Passenger Cars-Mechanical Systems*, vol. 1, no. 2008-01-0692, pp. 568–576, 2008.

[15] R. Isermann and M. Münchhof, *Identification of dynamic systems: an introduction with applications*. Springer, 2010.

[16] R. Tavares and M. Ruderman, "Energy harvesting using piezoelectric transducers for suspension systems," *Mechatronics*, vol. 65, 2020.

[17] D. Roylance, *Mechanics of Materials: Introduction to Elasticity*. MIT Press, 2000.

[18] R. Tavares, J. Molina, M. Al Sakka, M. Dhaens, and M. Ruderman, "Modeling of an active torsion bar automotive suspension for ride comfort and energy analysis in standard road profiles," in *8th Symposium on Mechatronic Systems and 11th Symposium on Nonlinear Control Systems*. IFAC, 2019, pp. 181–186.

[19] P. Múčka, "Simulated road profiles according to ISO 8608 in vibration analysis," *Journal of Testing and Evaluation*, vol. 46, 01 2018.